

Crossover-model approach to QCD phase diagram, equation of state and susceptibilities in the 2+1 and 2+1+1 flavor systems

Akihisa Miyahara,^{1,*} Masahiro Ishii,^{1,†} Hiroaki Kouno,^{2,‡} and Masanobu Yahiro^{1,§}

¹*Department of Physics, Graduate School of Sciences, Kyushu University, Fukuoka 819-0395, Japan*

²*Department of Physics, Saga University, Saga 840-8502, Japan*

(Dated: June 16, 2022)

We construct a simple model for describing the hadron-quark crossover transition by using lattice QCD (LQCD) data in the 2+1 flavor system, and draw the phase diagram in the 2+1 and 2+1+1 flavor systems through analyses of the equation of state (EoS) and the susceptibilities. In the present hadron-quark crossover (HQC) model, the entropy density s is defined by $s = f_H s_H + (1 - f_H) s_Q$ with the hadron-production probability f_H , where s_H is calculated by the hadron resonance gas model valid in low temperature (T) and s_Q is evaluated by the independent quark model that explains LQCD data on the EoS in a wide range $400 \lesssim T \lesssim 1000$ MeV. The f_H is determined from LQCD data on s and susceptibilities for the baryon-number (B), the isospin (I) and the hypercharge (Y) in the 2+1 flavor system. The HQC model is successful in reproducing LQCD data on the EoS and the flavor susceptibilities $\chi_{ff'}^{(2)}$ for $f, f' = u, d, s$ in the 2+1+1 flavor system, without changing the f_H . We define the hadron-quark transition temperature with $f_H = 1/2$. For the 2+1 flavor system, the transition line thus obtained is almost identical in μ_B-T , μ_I-T , μ_Y-T planes, when the chemical potentials μ_α ($\alpha = B, I, Y$) are smaller than 250 MeV. This BIY approximate equivalence persists also in the 2+1+1 flavor system. We plot the phase diagram also in μ_u-T , μ_d-T , μ_s-T , μ_c-T planes in order to investigate flavor dependence of transition lines. In the 2+1+1 flavor system, c quark does not affect the 2+1 flavor subsystem composed of u, d, s . The flavor off-diagonal susceptibilities are good indicators to see how hadrons survive as T increases, since the independent quark model hardly contributes to them. T dependence of the off-diagonal susceptibilities and the f_H show that the transition region at $\mu_\alpha = 0$ is $170 \lesssim T \lesssim 400$ MeV for both the 2+1 and 2+1+1 flavor systems.

PACS numbers: 12.40.-y

I. INTRODUCTION

Lattice QCD (LQCD) is the first-principle calculation of QCD, and has been providing a lot of information on hot QCD. Recently, the continuum and thermodynamic limits were taken in 2+1 flavor LQCD simulations [1], and it was confirmed that the chiral and deconfinement transitions are crossover at zero chemical potential.

As an approach alternative to LQCD simulations, we can consider effective models. This approach is useful for the physical interpretation of LQCD data and the prediction of physical quantities that are difficult to calculate in LQCD simulations. Recently, the Polyakov-loop extended Nambu-Jona-Lasinio (PNJL) type models have been used extensively, since they can treat both the chiral and the deconfinement transitions [2–14]. In the PNJL-type models, the pseudocritical temperature of the deconfinement transition is almost equal to or lower than that of the chiral transition. For the 2 flavor system, the PNJL-type models well explain LQCD data [11–14], since the two transitions take place almost simultaneously in LQCD simulations. For the 2+1 flavor system, however, LQCD shows that the chiral-transition temperature is considerably lower than the deconfinement-transition one [1, 15]. For this reason, it is not easy for the PNJL-type models to ex-

plain the chiral and deconfinement transitions simultaneously. It is thus important to construct a reasonable effective model for the 2+1 flavor system.

Now our discussion moves to the 2+1 flavor system composed of up (u), down (d), strange (s) quarks. For low temperature (T), the hadron resonance gas (HRG) model reproduces LQCD data on the equation of state (EoS) and the baryon-number (B) susceptibility [16–18]. In addition, below the chiral-transition temperature, the absolute value of chiral condensate is explained by HRG+chiral perturbation theory (χ PT) [19]. Recently, it was reported that the HRG model also accounts for LQCD data on T dependence of the Polyakov loop [20]. These results suggest that the hadron degree of freedom is important in QCD phase transitions, although it is not treated explicitly in the PNJL-type models.

Recently, the EoS, the baryon-number susceptibilities $\chi_B^{(n)}$ ($n = 2 \sim 4$) and the isospin (I) susceptibility $\chi_I^{(2)}$ were well described by hadron-quark hybrid models [21, 22]. This model also reproduces qualitatively that the chiral-transition temperature is lower than the deconfinement-transition one [22]. In the hadron-quark hybrid model of Ref. [21], the pressure P is defined by

$$P = f(T, \{\mu_\alpha\}) P_H(T, \{\mu_\alpha\}) + [1 - f(T, \{\mu_\alpha\})] P_Q(T, \{\mu_\alpha\}), \quad (1)$$

where the μ_α are the chemical potentials of quantum numbers $\alpha = B, I$ and hypercharge Y . The hadron piece P_H is calculated by the HRG model with the excluded volume and the quark-gluon piece P_Q is evaluated with perturbative

*miyahara@email.phys.kyushu-u.ac.jp

†ishii@phys.kyushu-u.ac.jp

‡kounoh@cc.saga-u.ac.jp

§yahiro@phys.kyushu-u.ac.jp

QCD [21]. Here, the fraction factor $f(T, \{\mu_\alpha\})$ is determined so as to reproduce LQCD data on P and the interaction measure. The other thermal quantities are obtainable from P .

Alternatively, one can start with the entropy density

$$s = f_H(T, \{\mu_\alpha\}) s_H(T, \{\mu_\alpha\}) + [1 - f_H(T, \{\mu_\alpha\})] s_Q(T, \{\mu_\alpha\}) \quad (2)$$

and calculate the other thermal quantities from s [23]. As an advantage of this approach, T dependence of s cannot be free. In fact, the T dependence should satisfy the thermodynamic inequality and the Nernst's theorem [24]:

$$\left. \frac{\partial s(T, \{\mu_\alpha\})}{\partial T} \right|_{\{\mu_\alpha\}=0} > 0, \quad s(T, \{\mu_\alpha\})|_{T=\{\mu_\alpha\}=0} = 0. \quad (3)$$

In this paper, this condition is automatically satisfied, since we use LQCD data as s . In Eq. (2), the factor f_H means the hadron-production probability. When $f_H(T, \{\mu_\alpha\}) = 1$ (0), the system is in the hadron (quark) phase composed of hadron (quark-gluon) matter only. In principle, the factor f_H is determinable from LQCD data on s , if s_H and s_Q are given. The hadron-quark hybrid model of Ref. [22] takes Eq. (2), and the hadron piece s_H is obtained by the HRG model and the quark-gluon piece s_Q is by the simple quark model in which an adjustable parameter is introduced so as to reproduce LQCD data [25] on $s(T, 0)$ at $T = 300$ MeV. The quark model is a simplified version of PNJL model: Namely, this model takes account of the coupling between the quark field and the homogeneous classical gauge field, but does not treat the quark-quark couplings that are not important above the chiral- and deconfinement-transition temperatures. We refer to the simple model as "independent quark (IQ) model" and the hadron-quark hybrid model of Ref. [22] as "hadron-quark crossover (HQC) model" in this paper.

Lately, state-of-art LQCD data on the EoS and the flavor diagonal and off-diagonal susceptibilities, $\chi_{ff'}$, became available for the 2+1+1 flavor system [25, 26] in addition to the case of the 2+1 flavor system [25, 27], where $f=u, d, s$ for the 2+1 system and $f=u, d, s, \text{charm } (c)$ for the 2+1+1 flavor system. It is an interesting question how c quark behaves in the 2+1+1 flavor system.

When the current quark mass m is infinity, Z_3 symmetry is exact and the Polyakov loop is an order parameter of the spontaneous Z_3 symmetry breaking. Dynamical quark with finite m breaks Z_3 symmetry explicitly through the temporal boundary condition for quark. For the 2+1 and 2+1+1 flavor systems, it is not clear that the Polyakov loop is still a good order parameter of the confinement-deconfinement (hadron-quark) transition. As a reasonable assumption, we define the hadron-quark transition temperature by $f_H = 1/2$. Another interesting question is how the phase diagram is in μ_B-T , μ_I-T , μ_Y-T planes and also in μ_u-T , μ_d-T , μ_s-T , μ_c-T planes, where μ_f ($f=u, d, s, c$) is the chemical potential for f quark.

In this paper, we reconstruct the HQC model by using new LQCD data [25, 27] in the 2+1 flavor system, and draw the phase diagram in the 2+1 and 2+1+1 flavor systems through analyses of the equation of state (EoS) and the susceptibilities.

In the previous work of Ref. [22], the IQ model had the momentum cutoff Λ_T in the thermal quark-loop term of P_Q . The cutoff Λ_T was introduced as an adjustable parameter to reproduce LQCD data [28] on s at $T = 300$ MeV, where the data were available in $T \leq 400$ MeV. Recently, however, we found that the IQ model begins to underestimate new LQCD data [25] as T increases from 400 MeV; here, LQCD data on s were deduced from new LQCD data [25] on P by differentiating P with respect to T and thereby LQCD data on s became available in $T \leq 500$ MeV. We then reformulate the IQ model slightly so that the model can explain the data in $400 \leq T \leq 1000$ MeV where the data is consistent with NNLO hard thermal loop (HTL) perturbation [29].

In the HQC model, $f_H(T, \{\mu_\alpha\})$ is determined from LQCD data on s , the baryon-number susceptibility $\chi_B^{(2)}$, the isospin susceptibility $\chi_I^{(2)}$ and the hypercharge (Y) susceptibility $\chi_Y^{(2)}$ in the 2+1 flavor system, where $\alpha = B, I, Y$. The HQC model with the $f_H(T, \{\mu_\alpha\})$ automatically reproduces LQCD data on the EoS and the $\chi_{ff'}^{(2)}$ in the 2+1 flavor system. In particular, the off-diagonal susceptibilities $\chi_{ff'}^{(2)}$ ($f \neq f'$) are good indicators to see how hadrons survive as T increases, since the IQ model hardly contributes to the off-diagonal susceptibilities [30]. In practice, the upper limit of the transition region is clearly determined by the off-diagonal susceptibilities. We then determine the transition region for the 2+1 flavor system with zero chemical potential from T dependence of $f_H(T, 0)$ and the off-diagonal susceptibilities.

Next, we draw the phase diagram in μ_B-T , μ_I-T , μ_Y-T planes. The transition lines are almost identical in these planes, when $\mu_\alpha < 250$ MeV. This property is referred to as "BIY approximate equivalence" in this paper. What is the nature of BIY approximate equivalence? This is discussed. We also plot the phase diagram in μ_u-T , μ_d-T , μ_s-T planes to see flavor dependence of hadron-quark transition lines.

The HQC model is applied to the EoS and the $\chi_{ff'}$ in the 2+1+1 flavor system without changing the $f_H(T, \{\mu_\alpha\})$. The HQC model succeeds in reproducing LQCD data on the EoS and the $\chi_{ff'}^{(2)}$ for $f, f'=u, d, s$, and explains $\chi_{cc}^{(2)}$ qualitatively. We then determine the transition region for the 2+1+1 flavor system with zero chemical potential from T dependence of $f_H(T, 0)$ and the off-diagonal susceptibilities, and investigate the role of c quark in the 2+1+1 flavor system.

Finally, we draw the phase diagram in μ_B-T , μ_I-T , μ_Y-T , μ_u-T planes to see whether BIY approximate equivalence persists in the 2+1+1 flavor system, and plot the diagram in μ_u-T , μ_d-T , μ_s-T , μ_c-T planes to investigate flavor dependence of hadron-quark transition lines.

This paper is organized as follows. In Sec. II, we recapitulate the HRG model and reformulate the IQ model without the cutoff Λ_T . We review the HQC model. Numerical results are shown in Sec III. Section IV is devoted to summary.

II. MODEL BUILDING

We reformulate the hadron-quark crossover (HQC) model of Ref. [22]. This model consists of the hadron resonance gas

(HRG) model reliable for small T and the independent quark (IQ) model reasonable for large T .

For later convenience, we define several kinds of chemical potentials. For the 2+1 flavor system, we represent the chemical potentials of u, d, s quarks by μ_u, μ_d and μ_s , respectively. These potentials are related to the baryon-number (B) chemical potential μ_B , the isospin (I) chemical potential μ_I and the hypercharge (Y) chemical potential μ_Y as

$$\begin{aligned}\mu_B &= \mu_u + \mu_d + \mu_s, \\ \mu_I &= \mu_u - \mu_d, \\ \mu_Y &= \frac{1}{2}(\mu_u + \mu_d - 2\mu_s)\end{aligned}\quad (4)$$

for the 2+1 flavor system. As for μ_I and μ_Y , the right-hand side of Eq. (4) stems from the diagonal elements of the matrix representation of Cartan algebra in the special unitary group $SU(3)$; namely, $\mu_I = (1, -1, 0)(\mu_u, \mu_d, \mu_s)^t$ and $\mu_Y = (1/2)(1, 1, -2)(\mu_u, \mu_d, \mu_s)^t$. Equation (4) gives

$$\begin{aligned}\mu_u &= \frac{1}{3}\mu_B + \frac{1}{2}\mu_I + \frac{1}{3}\mu_Y, \\ \mu_d &= \frac{1}{3}\mu_B - \frac{1}{2}\mu_I + \frac{1}{3}\mu_Y, \\ \mu_s &= \frac{1}{3}\mu_B - \frac{2}{3}\mu_Y.\end{aligned}\quad (5)$$

The coefficients on the right-hand side of Eq. (5) correspond to the quantum numbers of u, d, s quarks. In this sense, the definition (4) is natural.

Also in the 2+1+1 flavor system, we can define the following relations by using Cartan algebra in the special unitary group $SU(4)$ for μ_I, μ_Y and μ_{Y_c} :

$$\begin{aligned}\mu_B &= \frac{3}{4}(\mu_u + \mu_d + \mu_s + \mu_c), \\ \mu_I &= \mu_u - \mu_d, \\ \mu_Y &= \frac{1}{2}(\mu_u + \mu_d - 2\mu_s), \\ \mu_{Y_c} &= \frac{1}{3}(\mu_u + \mu_d + \mu_s - 3\mu_c),\end{aligned}\quad (6)$$

where the quantum number Y_c has been defined by $Y_c = (3/4)B - C$ with charmness C . Equation (6) leads to

$$\begin{aligned}\mu_u &= \frac{1}{3}\mu_B + \frac{1}{2}\mu_I + \frac{1}{3}\mu_Y + \frac{1}{4}\mu_{Y_c}, \\ \mu_d &= \frac{1}{3}\mu_B - \frac{1}{2}\mu_I + \frac{1}{3}\mu_Y + \frac{1}{4}\mu_{Y_c}, \\ \mu_s &= \frac{1}{3}\mu_B - \frac{2}{3}\mu_Y + \frac{1}{4}\mu_{Y_c}, \\ \mu_c &= \frac{1}{3}\mu_B - \frac{3}{4}\mu_{Y_c}.\end{aligned}\quad (7)$$

This final form is also natural, since the coefficients on the right-hand side of Eq. (7) are the quantum numbers of u, d, s, c quarks. Equation (6) is thus a natural extension of Eq. (4).

A. Hadron resonance gas model

For the hadron phase at low T , we use the HRG model. In the HRG model, the thermodynamic potential density Ω_H is described by free hadron gases. For convenience, Ω_H is divided into the baryonic piece Ω_B and the mesonic one Ω_M :

$$\Omega_H = \Omega_B + \Omega_M \quad (8)$$

with

$$\begin{aligned}\Omega_B &= - \sum_{i \in \text{Baryon}} d_{B,i} T \int \frac{d^3 \mathbf{p}}{(2\pi)^3} \{ \log(1 + e^{-(E_{B,i} - \mu_{B,i})/T}) \\ &\quad + \log(1 + e^{-(E_{B,i} + \mu_{B,i})/T}) \}\end{aligned}\quad (9)$$

and

$$\begin{aligned}\Omega_M &= \sum_{j \in \text{Meson}} d_{M,j} T \int \frac{d^3 \mathbf{p}}{(2\pi)^3} \{ \log(1 - e^{-(E_{M,j} - \mu_{M,j})/T}) \\ &\quad + \log(1 - e^{-(E_{M,j} + \mu_{M,j})/T}) \}\end{aligned}\quad (10)$$

for $E_{B,i} = \sqrt{\mathbf{p}^2 + m_{B,i}^2}$ and $E_{M,j} = \sqrt{\mathbf{p}^2 + m_{M,j}^2}$. Here, $m_{B,i}$ ($m_{M,j}$) and $\mu_{B,i}$ ($\mu_{M,j}$) is the mass and the chemical potential of the i -th baryon (j -th meson), respectively. In Eqs. (9) and (10), all the hadrons listed in the Particle Data Table [31] are taken; note that hadrons composed of u, d, s (u, d, s, c) quarks are picked up for the 2+1 (2+1+1) flavor system. The pressure P_H and the entropy density s_H are obtained from Ω_H as

$$P_H = P_B + P_M; \quad P_B = -\Omega_B, \quad P_M = -\Omega_M, \quad (11)$$

$$s_H = s_B + s_M; \quad s_B = \frac{\partial P_B}{\partial T}, \quad s_M = \frac{\partial P_M}{\partial T}. \quad (12)$$

Figure 1 shows the entropy density s and the pressure P as a function of T for the 2+1 flavor system with zero chemical potential. The HRG model (dotted line) well reproduces LQCD data [25, 28] in $T \lesssim 170$ MeV for s and $T \lesssim 190$ MeV for P . The hadron phase is thus realized in $T \lesssim 170$ MeV.

Figure 2 is the same as Fig. 1, but for 2+1+1 flavor system with zero chemical potential. The HRG model well explains LQCD data [25] in $T \lesssim 190$ MeV for the pressure and $T \lesssim 170$ MeV for the entropy density. We find from Fig. 2 that the hadron phase is realized in $T \lesssim 170$ MeV.

B. Independent quark model

Next, we consider the quark phase that may appear in the region $T \gtrsim 400$ MeV where LQCD data is consistent with NNLO HTL perturbation [29]. As shown later in Fig. 3, the entropy density calculated with LQCD simulations is about 80% of the Stefan-Boltzmann limit value even at $T = 1000$ MeV. This means that the massless ideal-gas (massless-free-particle) model does not work. For this reason, we consider the PNJL model without any quark-quark direct interactions, since the interactions are not important above the hadron-quark transition temperature. In the model, quarks interact with the gluon field A_μ by the gauge coupling g , but the spatial parts A_i ($i = 1, 2, 3$) are neglected and only the temporal part A_0 is treated as a stationary and uniform background field. In this sense, we call this model ‘‘independent quark (IQ) model’’.

As the gluonic action, we take the Polyakov-loop potential \mathcal{U} used in the PNJL model. The Lagrangian density of this

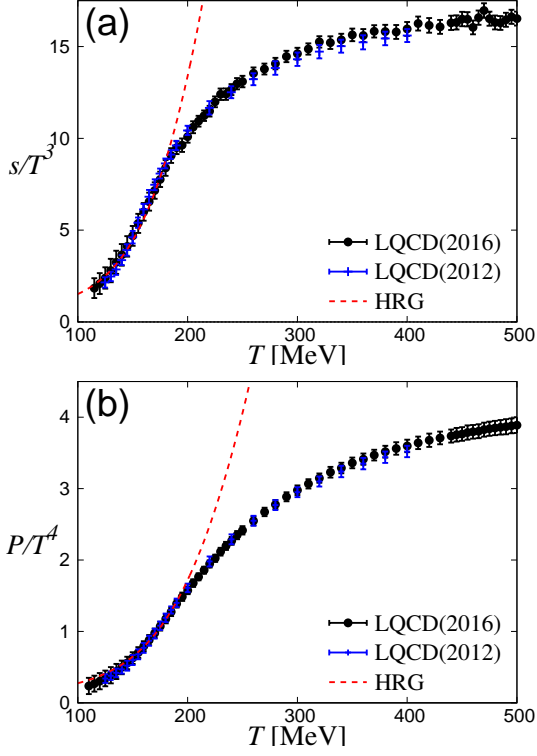


Fig. 1: T dependence of (a) the entropy density s and (b) the pressure P in the 2+1 flavor system with zero chemical potential. The dotted line means the result of the HRG model. LQCD data are taken from Refs. [25, 28]. In Ref. [25], LQCD data are available for P but not for s . The entropy density s is then evaluated by differentiating P with respect to T .

model is

$$\mathcal{L}_Q = \sum_f \{ \bar{q}_f (i\gamma^\mu D_\mu - m_f) q_f \} - \mathcal{U}(T, \Phi, \bar{\Phi}), \quad (13)$$

where m_f is the current mass of f quark and $D_\mu = \partial_\mu - igA_\mu^a \frac{\lambda_a}{2} \delta^{\mu 0}$ with the Gell-Mann matrix λ_a in color space. In Eq. (13), the q_f mean u, d, s quark fields for the 2+1 flavor system and u, d, s, c quark fields for the 2+1+1 flavor system. See Ref. [22] for the definition of the Polyakov-loop Φ and its conjugate $\bar{\Phi}$.

Making the path integral over quark fields, the Lagrangian (13) yields the thermodynamic potential density,

$$\begin{aligned} \Omega_Q = & \mathcal{U}(T, \Phi, \bar{\Phi}) \\ & - 2 \sum_f \left[\int_{|\mathbf{p}| \leq \Lambda_T} \frac{d^3 \mathbf{p}}{(2\pi)^3} (T \log z_f^+ + T \log z_f^-) \right] \end{aligned} \quad (14)$$

for the quark matter. The functions z_f^+ and z_f^- are defined by

$$z_f^+ = 1 + 3\bar{\Phi} e^{-(E_f + \mu_f)/T} + 3\Phi e^{-2(E_f + \mu_f)/T} + e^{-3(E_f + \mu_f)/T}, \quad (15)$$

$$z_f^- = 1 + 3\Phi e^{-(E_f - \mu_f)/T} + 3\bar{\Phi} e^{-2(E_f - \mu_f)/T} + e^{-3(E_f - \mu_f)/T} \quad (16)$$

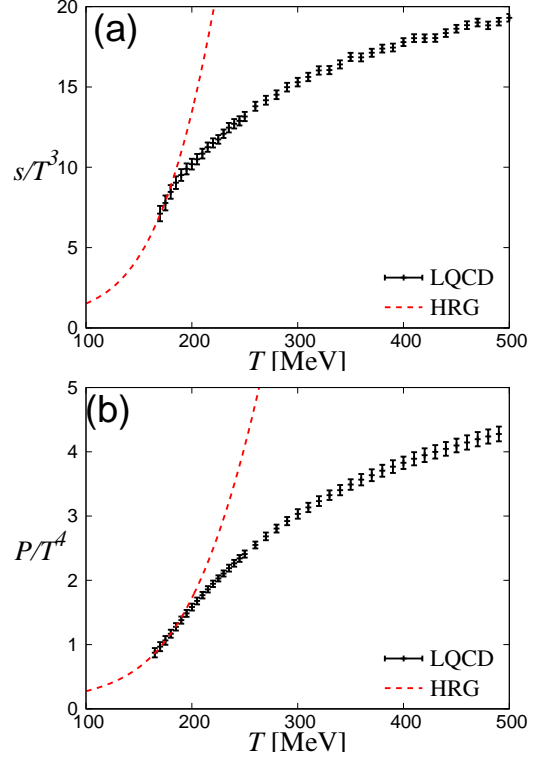


Fig. 2: T dependence of (a) the entropy density s and (b) the pressure P in the 2+1+1 flavor system with zero chemical potential. The dotted line means the result of the HRG model. In Ref. [25], LQCD data are available for P but not for s . The entropy density s is then evaluated by differentiating P with respect to T .

with $E_f = \sqrt{\mathbf{p}^2 + m_f^2}$. In Eq. (14), the vacuum term has been omitted, since the pressure calculated with LQCD simulations does not include the term. The pressure P_Q and the entropy density s_Q are obtained from Ω_Q as

$$P_Q = -\Omega_Q, \quad (17)$$

$$s_Q = \frac{\partial P_Q}{\partial T}. \quad (18)$$

We take the Polyakov-loop potential of Ref. [7]:

$$\begin{aligned} \frac{\mathcal{U}(T, \Phi, \bar{\Phi})}{T^4} = & -\frac{a(T)}{2} \Phi \bar{\Phi} \\ & + b(T) \log \{ 1 - 6\Phi \bar{\Phi} + 4(\Phi^3 + \bar{\Phi}^3) - 3(\Phi \bar{\Phi})^2 \}; \end{aligned} \quad (19)$$

$$a(T) = a_0 + a_1 \left(\frac{T_0}{T} \right) + a_2 \left(\frac{T_0}{T} \right)^2, \quad (20)$$

$$b(T) = b_3 \left(\frac{T_0}{T} \right)^3. \quad (21)$$

In Ref. [7], the parameters a_0, a_1, a_2, b_3 and T_0 were fitted to LQCD data on the EoS in the pure gauge theory. In high T , the potential is dominated by the a_0 term. For this reason, the value of $a_0/2$ is set to the Stefan-Boltzmann limit value ($a_0 = 3.51$) in the pure gauge theory, but the \mathcal{U} thus obtained overestimates new LQCD data [32] in $400 \leq T \leq 1000$ MeV.

In the 2+1 flavor system with dynamical quarks, furthermore, the quarks may change the Polyakov-loop potential. In fact, even at high T such as $T = 1000$ MeV, the pressure P calculated with LQCD simulations [33] is about 80 % of the Stefan-Boltzmann limit value in 2+1 flavor system; see for example Fig. 3. The entropy density, obtained by differentiating P with respect to T , also has the same property. This point is discussed below.

In our previous work of Ref. [22] for the 2+1 flavor system, the momentum cutoff Λ_T in the thermal quark-loop term of Ω_Q was determined to reproduce LQCD data [28] on s at $T = 300$ MeV, where the data were available in $T \leq 400$ MeV. However, we found that the model result with the resulting value $\Lambda_T = 1.95$ GeV begins to underestimate new LQCD data [25] as T increases from 400 MeV; here, we have evaluated the LQCD data on s from new data [25] on P measured in $T \leq 500$ MeV by differentiating P with respect to T . For this reason, we do not introduce Λ_T in this paper: Namely, $\Lambda_T = \infty$. As mentioned above, in the 2+1 flavor system, the entropy density s calculated with LQCD simulations underestimates the Stefan-Boltzmann limit value by about 20 % even at $T = 1000$ MeV. We then change the parameter a_0 so that the model result can reproduce the LQCD data at $T = 400$ MeV. The resulting value is $a_0 = 0.7 \times 3.51 = 2.457$; see Table I for the values of parameters in \mathcal{U} . The model result with $a_0 = 2.457$ well explains LQCD data on s in $400 \leq T \leq 1000$ MeV, as shown below. For the 2+1+1 flavor system, we keep $a_0 = 2.457$ to hold the simplicity of model.

a_0	a_1	a_2	b_3	T_0
2.457	-2.47	15.2	-1.75	270[MeV]

TABLE I: Parameters in the Polyakov-loop potential.

Figure 3 shows the entropy density s and the pressure P as a function of T for the 2+1 flavor system with zero chemical potential. LQCD data of Ref. [33] are improved in Ref. [25] with larger lattice. The pressure P was calculated in $T \leq 1000$ MeV for the first simulation, but in $T < 500$ MeV for the second simulation. Since the first data is smaller than the second one by about 5% at $T = 500$ MeV, we have then multiplied the first data by 1.05. For both the data, the entropy densities s have been obtained by differentiating P with respect to T . LQCD data are smaller than the result of the ideal-gas model (the Stefan-Boltzmann limit; dotted line) by about 20% even at $T = 1000$ MeV. The IQ model with the original value $a_0 = 3.51$ (dashed line) almost reaches the Stefan-Boltzmann limit at $T = 1000$ MeV. Meanwhile, the model with $a_0 = 2.457$ (solid line) well explains LQCD data in a wide range of $400 \leq T \leq 1000$ MeV. Thus, the quark phase may be realized in $T \gtrsim 400$ MeV. The lower limit of the quark phase is determinable clearly with T dependence of $\chi_{ff'}^{(2)}$ ($f \neq f'$). This analysis will be made later in Sec. III.

Figure 4 shows the entropy density s and the pressure P as a function of T for the 2+1+1 flavor system with zero chemical potential. LQCD calculations were done for P in Ref. [25]. The entropy density s is evaluated from the data by differ-

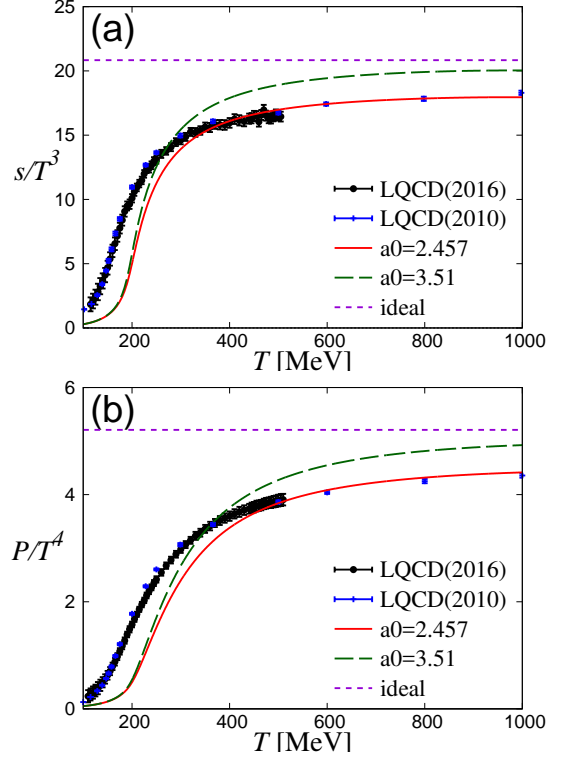


Fig. 3: T dependence of (a) the entropy density s and (b) the pressure P for the 2+1 flavor system with zero chemical potential. The dotted line is the result of the ideal-gas model (the Stefan-Boltzmann limit), the dashed line denotes the IQ model with the original value $a_0 = 3.51$, and the solid line corresponds to the IQ model with $a_0 = 2.457$. LQCD data of Ref. [25] (Ref. [33]) are denoted by dots (crosses); see the text for further explanation.

entiating P with respect to T . LQCD data are about 80% of the result of the ideal-gas model (the Stefan-Boltzmann limit; dotted line) at $T = 1000$ MeV. The IQ model with the original value $a_0 = 3.51$ (dashed line) reaches about 90% of the Stefan-Boltzmann limit value at $T = 1000$ MeV. The model with $a_0 = 2.457$ (solid line) reproduces LQCD data in $400 \leq T \leq 1000$ MeV pretty well. Thus, the quark phase may be realized in $T \gtrsim 400$ MeV also for the 2+1+1 flavor system. The lower limit of the quark phase can be determined precisely with T dependence of $\chi_{ff'}^{(2)}$ ($f \neq f'$). This analysis is also made in Sec. III.

C. Quark-hadron crossover model

Now we consider the HQC model defined by Eq. (2) in which $s_H(T, \{\mu_\alpha\})$ is calculated by the HRG model of Sec. II A and $s_Q(T, \{\mu_\alpha\})$ is by the IQ model of Sec. II B, where $\{\mu_\alpha\}$ means $\{\mu_B, \mu_I, \mu_Y\}$ for the 2+1 flavor system and $\{\mu_B, \mu_I, \mu_Y, \mu_{Y_c}\}$ for the 2+1+1 flavor system. This model is a natural extension of the model of Ref. [23] in which quarks and gluons are treated as ideal gases. The function $f_H(T, \{\mu_\alpha\})$ means the hadron-production probability. When $f_H(T, \{\mu_\alpha\}) = 1$ (0), the system consists of hadron matter

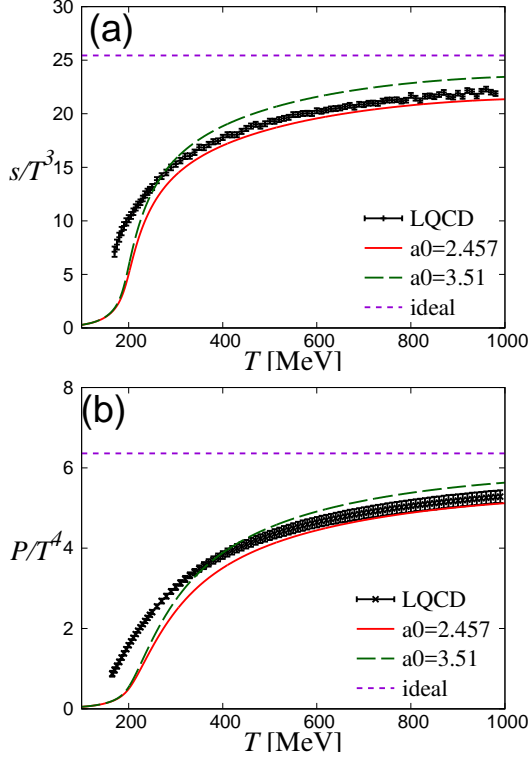


Fig. 4: T dependence of (a) the entropy density s and (b) the pressure P for the 2+1+1 flavor system with zero chemical potential. See Fig. 3 for the definition of lines. LQCD data (dots) are taken from Ref. [25]; see the text for further explanation.

(quark gluon matter) only, i.e., the system becomes the mixed phase in $0 < f_H(T, \{\mu_\alpha\}) < 1$.

In this paper, we consider $P(T)$ and $s(T)$ as the EoS and several kinds of second-order susceptibilities for the 2+1 and 2+1+1 flavor systems with zero chemical potential.

1. 2+1 flavor system

We recapitulate the formalism of Ref. [22]. For the 2+1 flavor system, the $f_H(T, \{\mu_\alpha\})$ is expanded into a power series of $\{\mu_\alpha\}$ and is taken up to the second order:

$$\begin{aligned}
 f_H(T, \{\mu_\alpha\}) = & f_H^{(0)}(T) + f_{H,B}^{(2)}(T) \left(\frac{\mu_B}{T_c} \right)^2 \\
 & + f_{H,I}^{(2)}(T) \left(\frac{\mu_I}{T_c} \right)^2 + f_{H,Y}^{(2)}(T) \left(\frac{\mu_Y}{T_c} \right)^2 \\
 & + f_{H,BY}^{(2)}(T) \left(\frac{\mu_B}{T_c} \right) \left(\frac{\mu_Y}{T_c} \right).
 \end{aligned} \quad (22)$$

where $T_c = 170$ MeV [19, 34] is the hadron-quark transition temperature defined with the Polyakov loop. The form of Eq. (22) comes from two properties; (i) s is invariant under charge conjugation, i.e., the transformation $(\mu_B, \mu_I, \mu_Y) \rightarrow (-\mu_B, -\mu_I, -\mu_Y)$, and (ii) the system is

also invariant under the interchange $\mu_u \leftrightarrow \mu_d$, i.e., the transformation $(\mu_B, \mu_I, \mu_Y) \rightarrow (\mu_B, -\mu_I, \mu_Y)$. For $\mu_B = \mu_I = \mu_Y = 0$, Eq. (2) reduces to

$$s(T) = f_H^{(0)}(T) s_H(T) + \{1 - f_H^{(0)}(T)\} s_Q(T). \quad (23)$$

The pressure P with no vacuum contribution is obtainable from s as

$$\begin{aligned}
 P(T, \{\mu_\alpha\}) &= \int_0^T dT' s(T', \{\mu_\alpha\}) \\
 &= \int_0^T dT' s_Q + \int_0^T dT' f_H (s_H - s_Q) \\
 &= P_Q(T, \{\mu_\alpha\}) + \int_0^T dT' f_H (s_H - s_Q). \quad (24)
 \end{aligned}$$

The second-order diagonal susceptibility $\chi_\alpha^{(2)}$ of quantum numbers $\alpha = B, I, Y$ is obtained as the second derivative of P with respect to the chemical potential μ_α :

$$\begin{aligned}
 \chi_\alpha^{(2)}(T, \{\mu_\alpha\}) &= \frac{\partial^2}{\partial \mu_\alpha^2} P(T, \{\mu_\alpha\}) \\
 &= \frac{\partial^2}{\partial \mu_\alpha^2} P_Q(T, \{\mu_\alpha\}) + \int_0^T dT' \left[\frac{\partial^2 f_H}{\partial \mu_\alpha^2} (s_H - s_Q) \right. \\
 &\quad \left. + 2 \frac{\partial f_H}{\partial \mu_\alpha} \frac{\partial (s_H - s_Q)}{\partial \mu_\alpha} + f_H \frac{\partial^2 (s_H - s_Q)}{\partial \mu_\alpha^2} \right]. \quad (25)
 \end{aligned}$$

Particularly at $\mu_B = \mu_I = \mu_Y = 0$, it becomes

$$\begin{aligned}
 \chi_\alpha^{(2)}(T) &= \frac{\partial^2}{\partial \mu_\alpha^2} P_Q(T, \{\mu_\alpha\})|_{\{\mu_\alpha\}=0} \\
 &\quad + \int_0^T dT' \left[2 f_{H,\alpha}^{(2)} (s_H - s_Q) + f_H^{(0)} \frac{\partial^2 (s_H - s_Q)}{\partial \mu_\alpha^2} \right]. \quad (26)
 \end{aligned}$$

Similarly, the BY correlation susceptibility is

$$\begin{aligned}
 \chi_{BY}^{(2)}(T, \{\mu_\alpha\}) &= \frac{\partial^2}{\partial \mu_B \partial \mu_Y} P(T, \{\mu_\alpha\}) \\
 &= \frac{\partial^2}{\partial \mu_B \partial \mu_Y} P_Q(T, \{\mu_\alpha\}) + \int_0^T dT' \left[\frac{\partial^2 f_H}{\partial \mu_B \partial \mu_Y} (s_H - s_Q) \right. \\
 &\quad + \frac{\partial f_H}{\partial \mu_B} \frac{\partial (s_H - s_Q)}{\partial \mu_Y} + \frac{\partial f_H}{\partial \mu_Y} \frac{\partial (s_H - s_Q)}{\partial \mu_B} \\
 &\quad \left. + f_H \frac{\partial^2 (s_H - s_Q)}{\partial \mu_B \partial \mu_Y} \right] \quad (27)
 \end{aligned}$$

for finite $\{\mu_\alpha\}$ and

$$\begin{aligned} & \chi_{BY}^{(2)}(T) \\ &= \frac{\partial^2}{\partial \mu_B \partial \mu_Y} P_Q(T, \{\mu_\alpha\})|_{\{\mu_\alpha\}=0} \\ &+ \int_0^T dT' \left[f_{H,BY}^{(2)}(s_H - s_Q) + f_H^{(0)} \frac{\partial^2 (s_H - s_Q)}{\partial \mu_B \partial \mu_Y} \right] \end{aligned} \quad (28)$$

for $\{\mu_\alpha\} = 0$.

Using Eqs. (23), (26), (28), one can determine $f_H^{(0)}$, $f_{H,\alpha}^{(2)}$, $f_{H,BY}^{(2)}$ from LQCD data on s , $\chi_\alpha^{(2)}$, $\chi_{BY}^{(2)}$ at $\{\mu_\alpha\} = 0$, respectively. Namely,

$$f_H^{(0)} = \frac{s^{\text{LQCD}} - s_Q}{s_H - s_Q} \quad (29)$$

and

$$\begin{aligned} f_{H,\gamma}^{(2)} &= \frac{1}{w(s_H - s_Q)} \left[\frac{\partial \chi_\gamma^{(2),\text{LQCD}}}{\partial T} - \frac{\partial \chi_\gamma^{(2),Q}}{\partial T} \right. \\ &\quad \left. - f_H^{(0)} \left(\frac{\partial \chi_\gamma^{(2),H}}{\partial T} - \frac{\partial \chi_\gamma^{(2),Q}}{\partial T} \right) \right] \end{aligned} \quad (30)$$

for $\gamma = \alpha, BY$, where the superscript ‘‘LQCD’’ means LQCD data, $w = 2$ for $\gamma = \alpha$ and $w = 1$ for $\gamma = BY$, and

$$\chi_\alpha^{(2),Q} = \frac{\partial^2 P_Q}{\partial \mu_\alpha^2} \Big|_{\{\mu_\alpha\}=0}, \quad \chi_{BY}^{(2),Q} = \frac{\partial^2 P_Q}{\partial \mu_B \partial \mu_Y} \Big|_{\{\mu_\alpha\}=0}. \quad (31)$$

Figure 5 shows the $f_H^{(0)}$ (dots with error bars) deduced from LQCD data [25] on s by using Eq. (29). We make the cubic spline interpolation for the mean values of data in order to obtain the smooth function that passes through the mean values. Here, the mean values have been taken in $175 \leq T \leq 400$ MeV where the mean values are smaller than 1, and have been set to 0 in $T > 400$ MeV where the mean values are quite small. In $T \leq 170$ MeV, LQCD data have large error bars and the mean values are not so reliable; in fact, the mean values are accidentally larger than 1 in $140 < T \leq 170$ MeV. For this reason, we have replaced the mean values by 1 in $T \leq 150$ MeV and have neglected the mean values in $150 < T \leq 170$ MeV. The smooth function thus obtained (solid line) is consistent with LQCD data; note that the function is very close to 1 in $150 < T \leq 170$ MeV. Figure 5 indicates that the mixed phase appears in a region $170 \leq T \leq 400$ MeV for the case of zero chemical potential. Here, it should be noted that in Eq. (2) the hadron piece $f_H s_H$ contributes to s up to 400 MeV since s_H increases rapidly as T increases. The upper limit of the phase transition can be determined clearly from the off-diagonal susceptibilities. This will be shown later in Sec. III A.

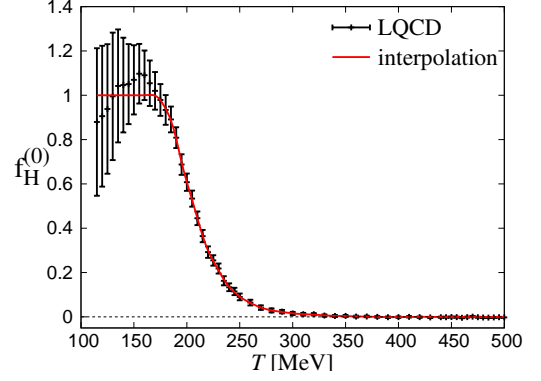


Fig. 5: T dependence of $f_H^{(0)}(T)$. The solid line is the smooth function obtained with the cubic spline interpolation. LQCD data on $f_H^{(0)}$ (dots) are deduced from those [25] on s by using Eq. (23).

Figure 6 shows $s(T)$ and $P(T)$ as a function of T in the case of zero chemical potential. The HQC model with the $f_H^{(0)}(T)$ determined above should reproduce LQCD data automatically. This is satisfied, as shown by the solid line.

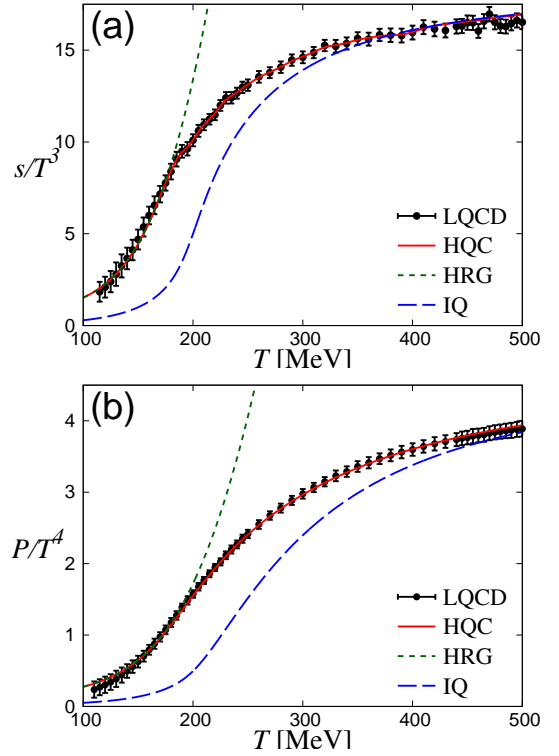


Fig. 6: T dependence of the entropy density s and the pressure P calculated by the HQC model for the 2+1 flavor system with zero chemical potential. The solid line is the HQC result based on the $f_H^{(0)}(T)$ determined in Fig. 5. The dotted line stands for the result of the HRG model, the dashed line corresponds to that of the IQ model. In Ref. [25], LQCD data are available for P but not for s . The entropy density s is then evaluated by differentiating P with respect to T .

We take the same procedure for $f_{H,\gamma}^{(2)}(T)$, where $\gamma =$

B, I, Y, BY . Namely, the $f_{H,\gamma}^{(2)}(T)$ are deduced from LQCD data [25] on $\chi_\gamma^{(2)}(T)$ by using Eq. (30), and the cubic spline interpolation is made for the mean values of the $f_{H,\gamma}^{(2)}(T)$. Here we have simply assumed $f_{H,\gamma}^{(2)}(T) = 0$ in $T \leq 127$ MeV where LQCD data are not available. The resulting smooth lines are plotted in Fig. 7. All the $f_{H,\gamma}^{(2)}(T)$ are order $\mathcal{O}(10^{-1})$. In order to confirm the accuracy of the cubic spline interpolation, we compare the original LQCD data on $\chi_\gamma^{(2)}(T)$ with the corresponding HQC result (solid line) in Fig. 8. As expected, good agreement is seen between them. Again, the HRG model (dotted line) reproduces the LQCD data in $T \leq 170$ MeV, while the IQ model well explains the data around $T = 400$ MeV.

One can see from Fig. 7 that the $f_{H,\gamma}^{(2)}(T)$ satisfy

$$f_{H,B}^{(2)}(T) \approx f_{H,Y}^{(2)}(T) \approx \frac{3}{4}f_{H,I}^{(2)}(T) \approx \frac{3}{4}f_{H,BY}^{(2)}(T) \quad (32)$$

around $T = 200$ MeV. The $f_{H,\gamma}^{(2)}(T)$ are thus close to each other around $T = 200$ MeV. This property plays an important role when we draw the QCD phase diagram in μ_B - T , μ_I - T , μ_Y - T planes. This will be discussed later in Sec. III A

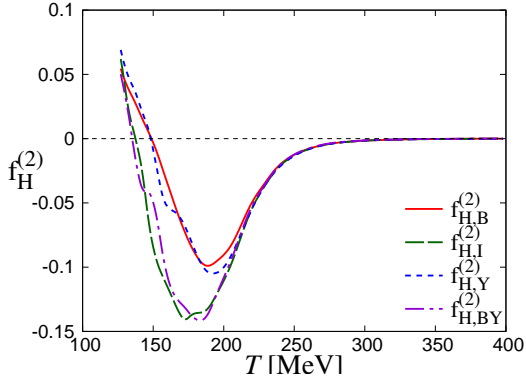


Fig. 7: Results of the cubic spline interpolation for T dependence of $f_{H,\gamma}^{(2)}$ that are deduced from LQCD data [25] on $\chi_\gamma^{(2)}$ by using Eq. (30). The results are plotted by the solid line for $f_{H,B}^{(2)}$, the dashed line for $f_{H,I}^{(2)}$, the dotted line for $f_{H,Y}^{(2)}$, and the dot-dashed line for $f_{H,BY}^{(2)}$.

Throughout the analyses mentioned above, we have succeeded in determining $f_H(T, \{\mu_\alpha\})$. The f_H can be described by μ_f ($f=u, d, s$) by using Eq. (4):

$$f_H(T, \{\mu_\alpha\}) = f_H^{(0)}(T) + \sum_{f,f' \in u,d,s} f_{H,ff'}^{(2)}(T) \left(\frac{\mu_f}{T_c} \right) \left(\frac{\mu_{f'}}{T_c} \right) \quad (33)$$

with

$$f_{H,uu}^{(2)}(T) = f_{H,B}^{(2)}(T) + f_{H,I}^{(2)}(T) + \frac{1}{4}f_{H,Y}^{(2)}(T) + \frac{1}{2}f_{H,BY}^{(2)}(T), \quad (34)$$

$$f_{H,ss}^{(2)}(T) = f_{H,B}^{(2)}(T) + f_{H,Y}^{(2)}(T) - f_{H,BY}^{(2)}(T), \quad (35)$$

$$f_{H,ud}^{(2)}(T) = 2f_{H,B}^{(2)}(T) - 2f_{H,I}^{(2)}(T) + \frac{1}{2}f_{H,Y}^{(2)}(T) + f_{H,BY}^{(2)}(T), \quad (36)$$

$$f_{H,us}^{(2)}(T) = 2f_{H,B}^{(2)}(T) - f_{H,Y}^{(2)}(T) - \frac{1}{2}f_{H,BY}^{(2)}(T); \quad (37)$$

note that $f_{H,uu}^{(2)}(T) = f_{H,dd}^{(2)}(T)$, $f_{H,ud}^{(2)}(T) = f_{H,du}^{(2)}(T)$ and $f_{H,us}^{(2)}(T) = f_{H,ds}^{(2)}(T)$.

Figure 9 shows T dependence of the $f_{H,ff'}^{(2)}$, that are derived from the $f_{H,\gamma}^{(2)}$ by using Eqs. (34)–(37). We can see from this figure that

$$f_{H,uu}^{(2)}(T) \approx 2.5f_{H,ud}^{(2)}(T) \approx 4f_{H,ss}^{(2)}(T) \approx 10f_{H,us}^{(2)}(T) \quad (38)$$

around $T = 200$ MeV. Thus, the s-quark contribution is small in the $f_{H,ff'}$, and also in the $f_{H,\gamma}$. This property induces the approximate relation $f_{H,B}^{(2)}(T) \approx f_{H,Y}^{(2)}(T)$ shown in Eq. (32), since

$$f_{H,B}^{(2)}(T) - f_{H,Y}^{(2)}(T) = \frac{1}{9} \left[-3f_{H,ss}^{(2)}(T) + 6f_{H,us}^{(2)}(T) \right] \approx 0. \quad (39)$$

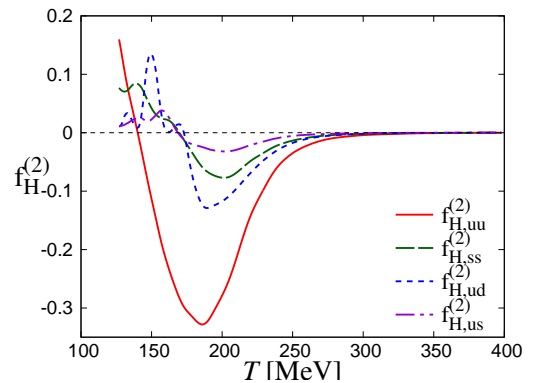


Fig. 9: T dependence of $f_{H,ff'}^{(2)}$ derived from $f_{H,\gamma}^{(2)}$. The results are plotted by the solid line for $f_{H,uu}^{(2)}$, the dashed line for $f_{H,ss}^{(2)}$, the dotted line for $f_{H,ud}^{(2)}$, and the dot-dashed line for $f_{H,us}^{(2)}$.

The flavor diagonal and off-diagonal susceptibilities $\chi_{ff'}^{(2)}(T, \{\mu_\alpha\})$ are obtained from P of Eq. (24) by using

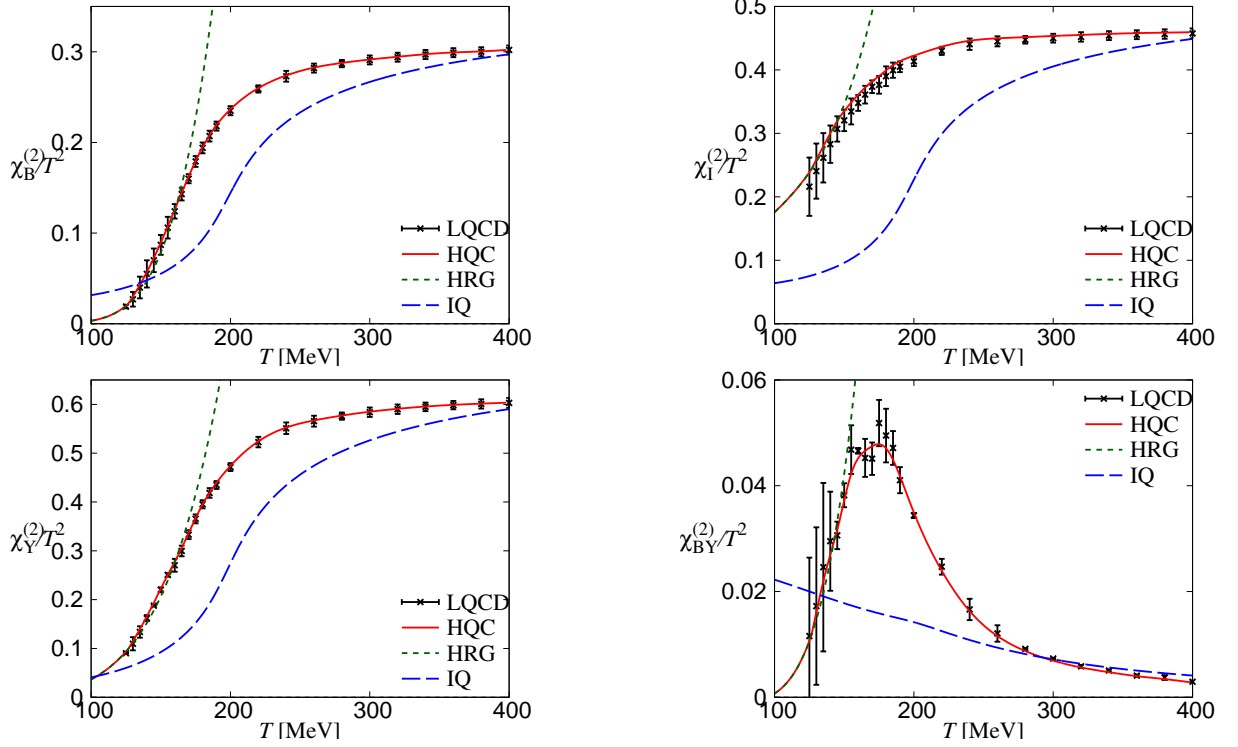


Fig. 8: T dependence of the baryon-number B and the isospin I , the hypercharge Y and the BY correlation susceptibility for the 2+1 flavor system with zero chemical potential. The HQC result is drawn by the solid line. The dotted line stands for the result of the HRG model, the dashed line corresponds to that of the IQ model. LQCD data (dots) are taken from Ref [25].

Eq. (33) as f_H :

$$\begin{aligned} & \chi_{ff'}^{(2)}(T, \{\mu_\alpha\}) \\ &= \frac{\partial^2}{\partial \mu_f \partial \mu_{f'}} P_Q(T, \{\mu_\alpha\}) \\ &+ \int_0^T dT' \left[\frac{\partial^2 f_H}{\partial \mu_f \partial \mu_{f'}} (s_H - s_Q) + \frac{\partial f_H}{\partial \mu_f} \frac{\partial (s_H - s_Q)}{\partial \mu_{f'}} \right. \\ &\left. + \frac{\partial f_H}{\partial \mu_{f'}} \frac{\partial (s_H - s_Q)}{\partial \mu_f} + f_H \frac{\partial^2 (s_H - s_Q)}{\partial \mu_f \partial \mu_{f'}} \right] \end{aligned} \quad (40)$$

for finite $\{\mu_\alpha\}$ and

$$\begin{aligned} & \chi_{ff'}^{(2)}(T) \\ &= \chi_{ff'}^{(2),Q}(T, \{\mu_\alpha\})|_{\{\mu_\alpha\}=0} \\ &+ \int_0^T dT' \left[w f_{H,ff'}^{(2)} (s_H - s_Q) + f_H^{(0)} \frac{\partial^2 (s_H - s_Q)}{\partial \mu_f \partial \mu_{f'}} \right] \end{aligned} \quad (41)$$

for $\{\mu_\alpha\} = 0$, where $w = 2$ for $f = f'$ and 1 for $f \neq f'$. It is known that the off-diagonal flavor susceptibilities $\chi_{ff'}^{(2),Q}(T)$ of the PNJL-type model are negligibly small [30]. Hence, for simplicity of calculation, we put $\chi_{ff'}^{(2),Q}(T) = 0$ for $f \neq f'$.

2. 2+1+1 flavor system

Also for the 2+1+1 flavor system, the hadron-production probability can be described by

$$\begin{aligned} & f_H^{2+1+1}(T, \{\mu_\alpha\}) \\ &= f_H^{2+1+1,(0)}(T) \\ &+ \sum_{f,f' \in u,d,s,c} f_{H,ff'}^{2+1+1,(2)}(T) \left(\frac{\mu_f}{T_c} \right) \left(\frac{\mu_{f'}}{T_c} \right). \end{aligned} \quad (42)$$

In order to keep the simplicity of our model, however, we assume that the f_H of Eq. (33) is applicable for the 2+1 flavor subsystem of the 2+1+1 flavor system, and that $f_{H,cf}^{2+1+1,(2)} = 0$ for $f = u, d, s, c$. In this case, the HQC model has no adjustable parameter for the 2+1+1 flavor system. This assumption is justified later in Sec. III B. The procedure for obtaining the EoS and the flavor diagonal and off-diagonal susceptibilities is the same as in the 2+1 flavor system. Hereafter, we neglect the superscript “2+1+1” in f_H^{2+1+1} , when it does not induce any confusion.

III. NUMERICAL RESULTS

A. 2+1 flavor system

In general, the pseudocritical temperature $T_c^{(\mathcal{O})}$ of hadron-quark (confinement-deconfinement) crossover depends on observable \mathcal{O} considered. The definition commonly used is the peak in the T derivative of the Polyakov loop Φ . Figure 10

shows T dependence of the Polyakov loop Φ . In the HQC model, Φ is calculated by the IQ model. LQCD data are available for the 2+1 flavor system [19, 34]. Our model (solid line) reproduces the LQCD data pretty well. The pseudocritical temperature $T_c^{(\Phi)} = 201$ MeV of our model is somewhat larger than LQCD result $T_c^{(\Phi), \text{LQCD}} = 170 \pm 7$ MeV. The model result (dashed line) for the 2+1+1 flavor system is very close to that (solid line) for the 2+1 flavor system. This indicates that c quark hardly affects the hadron-quark transition. In practice, this supports that the $f_H(T, \{\mu_\alpha\})$ determined from the 2+1 flavor LQCD data is applicable for the 2+1+1 flavor system, if we do not mind $\chi_{H,cf}^{(2)}$ ($f = u, d, s, c$).

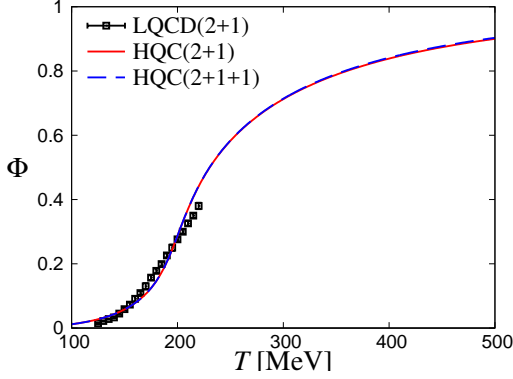


Fig. 10: T dependence of the Polyakov loop Φ in the 2+1 and 2+1+1 flavor systems with zero chemical potential. LQCD data are available for the 2+1 flavor system [19, 34]. The solid and dashed lines are results of our model for the 2+1 and 2+1+1 flavor systems, respectively.

As an alternative to $T_c^{(\Phi)}$, we may consider $f_H(T, \{\mu_\alpha\}) = 1/2$ as a definition of T_c . Our result is $T_c^{(f_H)} = 207$ MeV for $\{\mu_\alpha\} = 0$ and somewhat larger than the LQCD result $T_c^{(\Phi)} = 170 \pm 7$ MeV [19, 34].

Figure 11 shows the QCD phase diagram in μ_B - T , μ_I - T , μ_Y - T planes. The symbol $T_c(\mu_\alpha)$ denotes the pseudocritical temperature of the hadron-quark transition in μ_α - T plane, where the pseudocritical temperature is defined by $f_H = 1/2$. In virtue of Eq. (32), the three transition lines almost agree with each other. Thus, the relation

$$T_c(\mu_B) \approx T_c(\mu_I) \approx T_c(\mu_Y) \quad (43)$$

is satisfied in $\mu_\alpha < 250$ MeV. We call this relation “BIY approximate equivalence” in the present paper. As for the μ_B direction, we can evaluate the fourth-order term $f_{H,B}^{(4)}$ from LQCD data on $\chi_B^{(4)}$. We have confirmed that the $f_{H,B}^{(4)}$ does not affect $T_c(\mu_B)$ in $\mu_B < 250$ MeV.

BIY approximate equivalence comes from the property of Eq. (32). As already mentioned in Sec. II C 1, the approximate relation $f_{H,B}^{(2)}(T) \approx f_{H,Y}^{(2)}(T)$ in Eq. (32) comes from the fact that the s -quark contribution is small in the $f_{H,\gamma}^{(2)}(T)$ ($\gamma = B, I, Y, BY$). Meanwhile, the relation $f_{H,B}^{(2)}(T) \approx 3f_{H,Y}^{(2)}(T)/4$ in Eq. (32) is a remnant of the fact that in the

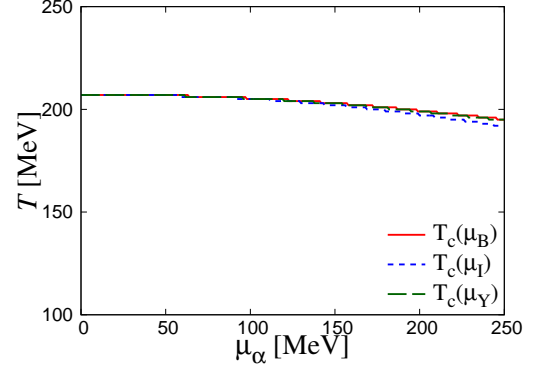


Fig. 11: Phase diagram in μ_B - T , μ_I - T , μ_Y - T planes.

2 flavor system $T_c(\mu_B) = T_c(\mu_I)$ when these are expressed up to $(\mu_\alpha/T)^2$ ($\alpha = B, I$) [35].

Next, we consider the flavor dependence of the pseudocritical temperature of the hadron-quark transition. Figure 12 shows the QCD phase diagram in μ_f - T planes. The symbol $T_c(\mu_f)$ denotes the pseudocritical temperature in μ_f - T plane. Note that $T_c(\mu_u) = T_c(\mu_d)$ for $\mu_u = \mu_d$, because of $f_{H,uu}^{(2)}(T) = f_{H,dd}^{(2)}(T)$ and $f_{H,us}^{(2)}(T) = f_{H,ds}^{(2)}(T)$. We then draw $T_c(\mu_u)$ and $T_c(\mu_s)$ only in Fig. 12. The transition takes place at higher T in μ_s - T plane than in μ_u - T plane. This may stem from the fact that $m_s \gg m_u = m_d$. Further discussion will be made in Sec. III B.

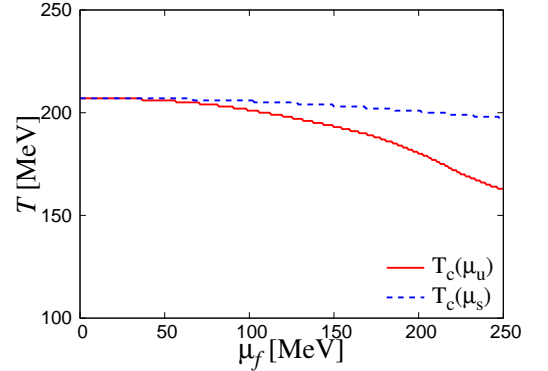


Fig. 12: Phase diagram in μ_u - T and μ_s - T planes. Note that $T_c(\mu_u) = T_c(\mu_d)$ $\mu_u = \mu_d$ because of $f_{H,uu}^{(2)}(T) = f_{H,dd}^{(2)}(T)$ and $f_{H,us}^{(2)}(T) = f_{H,ds}^{(2)}(T)$.

Figure 13 shows the flavor diagonal and off-diagonal susceptibilities, $\chi_{ff}^{(2)}$, as a function of T in the 2+1 flavor system with zero chemical potential. The solid line is the result of the HQC model. The HQC model should reproduce LQCD data on the $\chi_{ff}^{(2)}$ automatically. This is satisfied. Just for comparison, the results of the HRG and IQ models are denoted by dashed and dotted lines, respectively. As already mentioned in Sec. II C 1, the IQ model has no contribution for the off-diagonal susceptibilities. Noting $\chi_{ud}^{(2)} \approx 5\chi_{us}^{(2)}$, one can see from T dependence of the off-diagonal susceptibilities that most of hadrons disappear at $T = 400$ MeV. The hadron-quark transition thus ends up with $T \approx 400$ MeV.

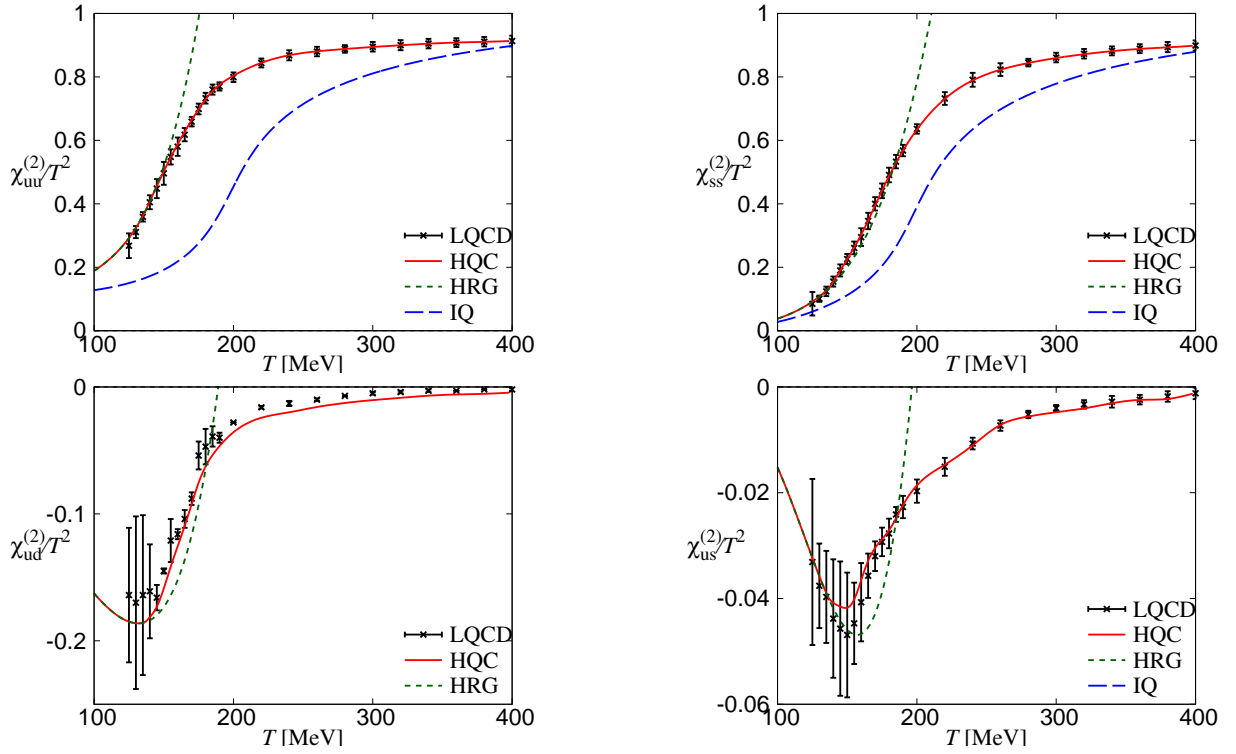


Fig. 13: T dependence of diagonal and off-diagonal susceptibilities, $\chi_{ff'}^{(2)}$, in the 2+1 flavor system with zero chemical potential. The HQC result is drawn by the solid line. The dotted line stands for the result of the HRG model, the dashed line corresponds to that of the IQ model. LQCD data are taken from Ref. [27].

B. 2+1+1 flavor system

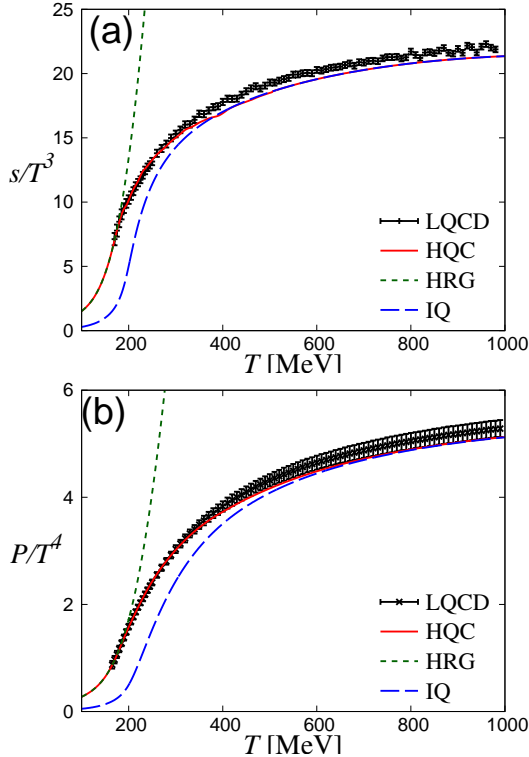


Fig. 14: T dependence of s and P in the 2+1+1 flavor system with zero chemical potential. The solid line is the result of the HQC model. LQCD data are taken from Ref. [25]. The result of the IQ (HRG) model is denoted by a dashed (dotted) line.

Figure 14 shows s and P as a function of T in the 2+1+1 flavor system with zero chemical potential. Good agreement is seen between the HQC results (solid line) and LQCD data. Comparing the HQC results with the HRG and IQ ones, we can see that the transition region is $170 \leq T \leq 400$ MeV. The upper limit of the phase transition can be determined more clearly with the off-diagonal susceptibilities, as shown below.

Figure 15 shows the flavor diagonal and off-diagonal susceptibilities, $\chi_{ff'}^{(2)}$, as a function of T in the 2+1+1 flavor system with zero chemical potential. One can see good agreement between LQCD data and the HQC results for the 2+1 flavor sector, i.e., $\chi_{uu}^{(2)}$, $\chi_{ud}^{(2)}$, $\chi_{ss}^{(2)}$, $\chi_{us}^{(2)}$. This supports the statement that c quark does not affect the 2+1 flavor subsystem composed of u, d, s quarks, together with the fact that $\chi_{uu}^{(2)}$, $\chi_{ud}^{(2)}$, $\chi_{ss}^{(2)}$, $\chi_{us}^{(2)}$ in the 2+1+1 flavor system are close to the corresponding susceptibilities in the 2+1 flavor system. Noting $\chi_{ud}^{(2)} \approx 5\chi_{us}^{(2)} \gg \chi_{uc}^{(2)}$, we can consider from T dependence of the off-diagonal susceptibilities that most of hadrons disappear at $T = 400$ MeV. Also for the 2+1+1 flavor system, the hadron-quark transition thus ends up with $T \approx 400$ MeV. Hence, the transition region is $170 \leq T \leq 400$ MeV also for the 2+1+1 flavor system with zero chemical potential.

The present HQC model neglects μ_c -dependence in $f_H(T, \{\mu_\alpha\})$, but reproduces LQCD data qualitatively for $\chi_{cc}^{(2)}$. As for $\chi_{uc}^{(2)}$, both LQCD and the HQC model show the correlation between u and c quarks is negligible in the transition region $170 \leq T \leq 400$ MeV.

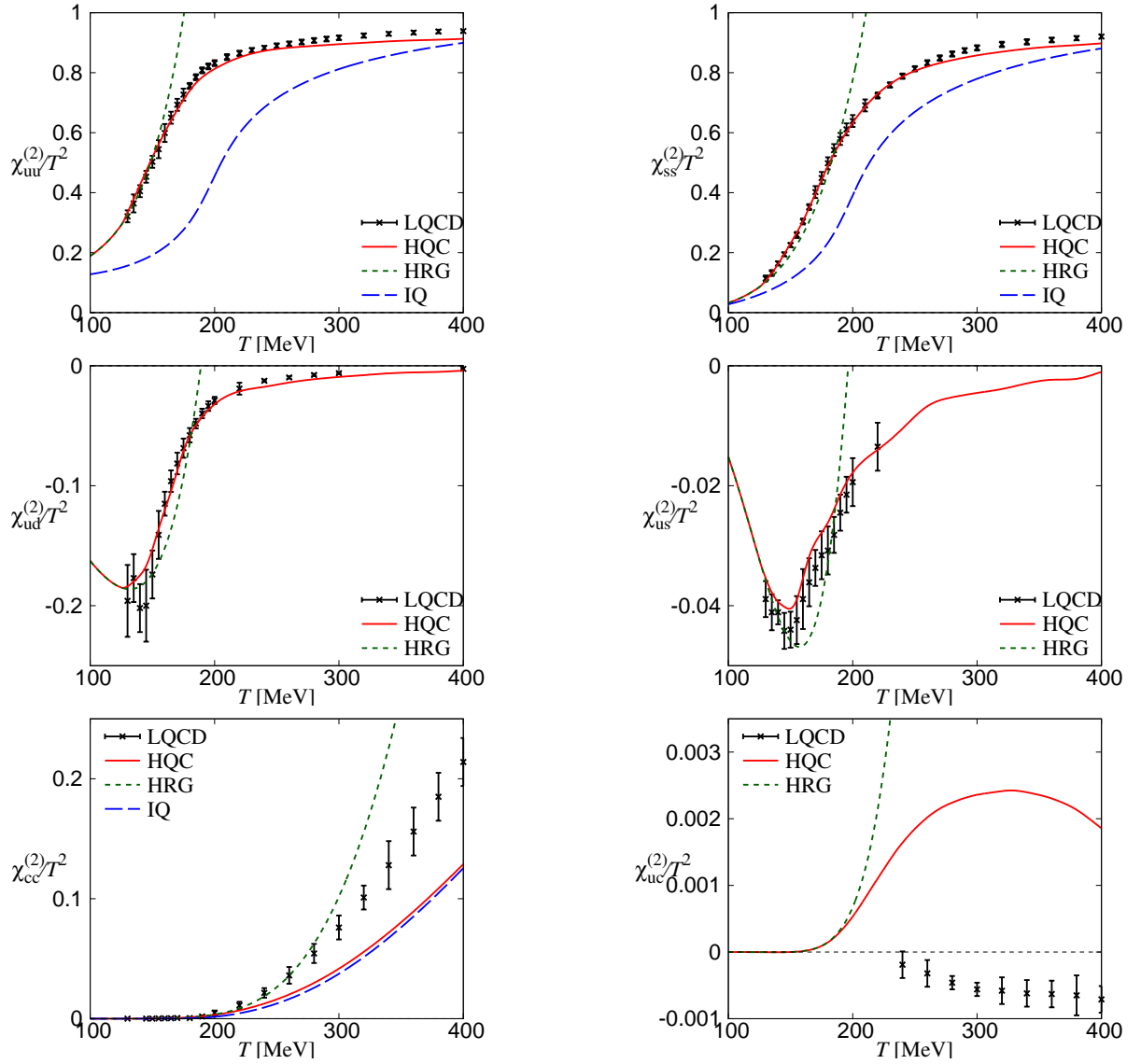


Fig. 15: T dependence of flavor diagonal and off-diagonal susceptibilities, $\chi_{ff}^{(2)}$, in the 2+1+1 flavor system with zero chemical potential. The solid line denotes the HQC result, while the chain line is the HRG result. The dotted line stands for the result of the HRG model, the dashed line corresponds to that of the IQ model. LQCD (dots) data are taken from Ref [25].

Finally, we discuss the phase diagram in μ_B - T , μ_I - T , μ_Y - T , μ_{Y_c} - T planes. For this purpose, we have evaluated $f_{H,cc}^{(2)}$ from $\chi_{cc}^{(2)}$, but $f_{H,cc}^{(2)} \approx f_{H,ss}^{(2)}/100$ around $T = 200$ MeV. This justifies our assumption that $f_{H,cc}^{(2)}$ is negligible in f_H , if we do not analyze $\chi_{cc}^{(2)}$ itself. Here, note that $f_{H,cu}^{(2)}$ is even smaller than $f_{H,cc}^{(2)}$. Using the assumption $f_{H,cu}^{(2)} = f_{H,su}^{(2)} = f_{H,cc}^{(2)} = 0$ in f_H , we draw the phase diagram in Fig. 16. *BIY* approximate equivalence still persists in the 2+1+1 flavor system, but the transition line $T_c(\mu_{Y_c})$ in μ_{Y_c} - T plane is slightly higher than in the other planes. This is because the difference, $f_{H,Y_c}^{(2)} - f_{H,B}^{(2)}$, has the $f_{H,uu}^{(2)}$ that is rather larger than the others around $T = 200$ MeV.

Figure 17 shows the phase diagram in μ_u - T , μ_d - T , μ_s -

T , μ_c - T planes; here note that $T_c(\mu_u) = T_c(\mu_d)$ when $\mu_u = \mu_d$. In this analysis, the transition line in μ_c - T plane is $T_c(\mu_c) = 207$ MeV, because of $f_{H,cc}^{(2)}(T) = 0$. We can find that $T_c(\mu_u) < T_c(\mu_s) < T_c(\mu_c)$ when $\mu_u = \mu_s = \mu_c$. This result indicates that the hadron-quark transition takes place at higher T for heavier quark. This is quite reasonable. In the nonrelativistic limit that is a good approximation for c quark, the QCD partition function is a function of $\mu_c - m_c$ and thereby the effect of μ_c is sizably reduced with large m_c .

IV. SUMMARY

We reconstructed the hadron-quark crossover (HQC) model of Ref. [22] by using new LQCD data [25, 27] in the 2+1 fla-

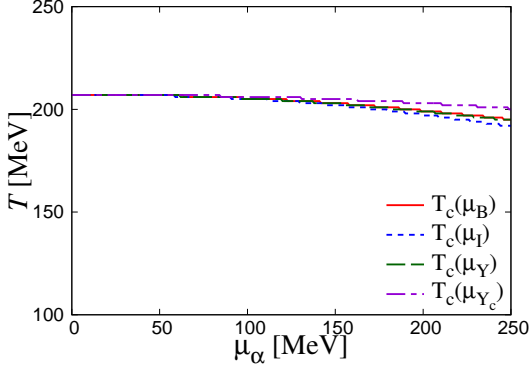


Fig. 16: Phase diagram in μ_B - T , μ_I - T , μ_Y - T , μ_{Y_c} - T planes.

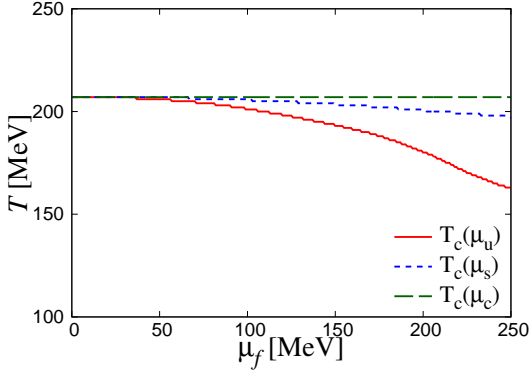


Fig. 17: Phase diagram in μ_u - T , μ_s - T , μ_c - T planes. Note that $T_c(\mu_u) = T_c(\mu_d)$ for $\mu_u = \mu_d$ because of $f_{H,uu}^{(2)}(T) = f_{H,dd}^{(2)}(T)$ and $f_{H,us}^{(2)}(T) = f_{H,ds}^{(2)}(T)$.

vor system, and we drew the phase diagram in the 2+1 and 2+1+1 flavor systems through analyses of the EoS and the susceptibilities.

The HQC model is defined by Eq. (2) in which $s_H(T, \{\mu_\alpha\})$ is calculated by the hadron resonance gas (HRG) model valid in low T and $s_Q(T, \{\mu_\alpha\})$ is by the independent quark (IQ) model reasonable in high T , where $\{\mu_\alpha\} = (\mu_B, \mu_I, \mu_Y)$. As mentioned above, the present version of the IQ model is rather reliable, since it explains LQCD data on the EoS in $400 \lesssim T \lesssim 1000$ MeV where LQCD data is consistent with NNLO HTL perturbation [29].

The hadron-production probability $f_H(T, \{\mu_\alpha\})$ was determined from LQCD data on s and the susceptibilities $\chi_\gamma^{(2)}$ for $\gamma = B, I, Y, BY$ in the 2+1 flavor system. Hence, the present HQC model automatically reproduces LQCD data on the EoS and the $\chi_{ff'}^{(2)}$ in the 2+1 flavor system. In particular, the off-diagonal susceptibilities $\chi_{ff'}^{(2)}$ ($f \neq f'$) are good indicators to see how hadrons survive as T increases, since the IQ model hardly contributes to the off-diagonal susceptibilities. In fact, the off-diagonal susceptibilities show that most of hadrons disappear above $T = 400$ MeV. In practice, the upper limit of the transition region is clearly determined by the off-diagonal susceptibilities. We then determined, from T dependence of

$f_H^{(0)}(T)$ and the off-diagonal susceptibilities, that the transition region is $170 \lesssim T \lesssim 400$ MeV for the 2+1 flavor system with zero chemical potential.

In the present paper, we defined the hadron-quark transition temperature by $f_H(T, \{\mu_\alpha\}) = 1/2$. For the 2+1 flavor system with zero chemical potential, the transition temperature is $T_c^{(f_H)} = 207$ MeV and somewhat larger than LQCD result $T_c^{(\Phi), \text{LQCD}} = 170 \pm 7$ MeV. This result $T_c^{(f_H)} = 207$ MeV is common between the 2+1 and 2+1+1 flavor systems, because $f_H^{(0)}(T)$ is the same between the two systems.

As mentioned above, the HQC model well simulates LQCD data on the EoS and the $\chi_{ff'}^{(2)}$ in the 2+1 flavor system. We then drew the phase diagram in μ_B - T , μ_I - T , μ_Y - T planes. We found “BIY approximate equivalence”: Namely, the transition lines $T_c(\mu_\alpha)$ are almost identical in these planes, when the μ_α are less than 250 MeV. The relation $T_c(\mu_B) \approx T_c(\mu_Y)$ comes from the fact that the s-quark contribution is small in the $f_{H,\gamma}^{(2)}(T)$ for $\gamma = B, I, Y, BY$. The relation $T_c(\mu_B) \approx T_c(\mu_I)$ may be a remnant of the fact that in the 2 flavor system $T_c(\mu_B) = T_c(\mu_I)$ when these are expressed up to $(\mu_B/T)^2$ and $(\mu_I/T)^2$ [35].

The HQC model was applied to the 2+1+1 flavor system without changing the f_H . The HQC model well reproduces LQCD data on the EoS and the $\chi_{ff'}^{(2)}$ for $f, f' = u, d, s$. This result indicates that transition region at $\{\mu_\alpha\} = 0$ is $170 \lesssim T \lesssim 400$ MeV also for the 2+1+1 flavor system, since between the 2+1 and 2+1+1 flavor systems the $f_H^{(0)}$ is the same and the $\chi_{ff'}^{(2)}$ for $f, f' = u, d, s$ are close to each other. In addition, T dependence of Φ is almost identical between the 2+1 and 2+1+1 flavor systems. These results show that c quark does not affect the 2+1 flavor subsystem composed of u, d, s quarks. This statement is supported by the fact that $\chi_{ud}^{(2)} \approx 5\chi_{us}^{(2)} \gg \chi_{uc}^{(2)}$ in the transition region.

The present HQC model has no μ_c -dependence in $f_H(T, \{\mu_\alpha\})$, but reproduces LQCD data qualitatively for $\chi_{cc}^{(2)}$. As for $\chi_{uc}^{(2)}$, both LQCD and the HQC model show the correlation between u and c quarks is negligible in the transition region $170 \lesssim T \lesssim 400$ MeV.

Finally, we plotted the phase diagram both in μ_B - T , μ_I - T , μ_Y - T , μ_{Y_c} - T planes and in μ_u - T , μ_d - T , μ_s - T , μ_c - T planes. BIY approximate equivalence still persists in the 2+1+1 flavor system, but the transition line $T_c(\mu_{Y_c})$ in μ_{Y_c} - T plane is slightly higher than in the other planes. We also found that $T_c(\mu_u) < T_c(\mu_s) < T_c(\mu_c)$ when $\mu_u = \mu_s = \mu_c$. This result indicates that the hadron-quark transition takes place at higher T for heavier quark. This is quite natural. In the non-relativistic limit that is a good approximation for c quark, the QCD partition function is a function of $\mu_c - m_c$, so that the effect of μ_c is greatly reduced with large m_c .

Acknowledgments

The authors thank Atsushi Nakamura, Kouji Kashiwa, Junichi Takahashi, Junpei Sugano, Shuichi Togawa, Yuhei Torigoe and Takehiro Hirakida for useful discussions. M. Y. and

H. K. were supported by Grant-in-Aid for Scientific Research (No. 26400278 and No. 26400279) from the Japan Society

for the Promotion of Science (JSPS).

-
- [1] Y. Aoki, G. Endrödi, Z. Fodor, S. D. Katz and K. K. Szabó, *Nature* **443**, 675 (2006).
 - [2] P. N. Meisinger, and M. C. Ogilvie, *Phys. Lett. B* **379**, 163 (1996).
 - [3] A. Dumitru, and R. D. Pisarski, *Phys. Rev. D* **66**, 096003 (2002).
 - [4] K. Fukushima, *Phys. Lett. B* **591**, 277 (2004); *Phys. Rev. D* **77**, 114028 (2008).
 - [5] C. Ratti, M. A. Thaler, and W. Weise, *Phys. Rev. D* **73**, 014019 (2006); C. Ratti, S. Röbner, M. A. Thaler, and W. Weise, *Eur. Phys. J. C* **49**, 213 (2007).
 - [6] E. Megias, E. Ruiz Arriola, and L. L. Salcedo, *Phys. Rev. D* **74**, 065005 (2006).
 - [7] S. Röbner, C. Ratti, and W. Weise, *Phys. Rev. D* **75**, 034007 (2007).
 - [8] B. -J. Schaefer, J. M. Pawłowski, and J. Wambach, *Phys. Rev. D* **76**, 074023 (2007).
 - [9] H. Abuki, R. Anglani, R. Gatto, G. Nardulli, and M. Ruggieri, *Phys. Rev. D* **78**, 034034 (2008).
 - [10] K. Kashiwa, H. Kouno, M. Matsuzaki, and M. Yahiro, *Phys. Lett. B* **662**, 26 (2008).
 - [11] Y. Sakai, T. Sasaki, H. Kouno, and M. Yahiro, *Phys. Rev. D* **82**, 076003 (2010).
 - [12] R. Gatto, and M. Ruggieri, *Phys. Rev. D* **83**, 034016 (2011).
 - [13] T. Sasaki, Y. Sakai, H. Kouno, and M. Yahiro, *Phys. Rev. D* **84**, 091901 (2011).
 - [14] K. Kashiwa, T. Hell, and W. Weise, *Phys. Rev. D* **84**, 056010 (2011).
 - [15] Y. Aoki, A. Fodor, S. D. Katz, and K. K. Szabó, *Phys. Lett. B* **643**, 46 (2006).
 - [16] S. Borsányi, Z. Fodor, C. Hoelbling, S. D. Katz, S. Krieg, C. Ratti, and K. K. Szabo, *arXiv:1005.3508 [hep-lat]* (2010).
 - [17] S. Borsányi, Z. Fodor, C. Hoelbling, S. D. Katz, S. Krieg, C. Ratti, and K. K. Szabo, *Phys. Lett. B* **730**, 99 (2014).
 - [18] J. Steinheimer, and S. Schramm, *[arXiv:1401.4051 [nucl-th]]* (2014).
 - [19] S. Borsányi, Z. Fodor, C. Hoelbling, S. D. Katz, S. Krieg, C. Ratti, and K. K. Szabo, *JHEP* **09**, 073 (2010).
 - [20] E. Megias, E. Ruiz Arriola, and L. L. Salcedo, *Phys. Rev. Lett.* **109**, 151601 (2012).
 - [21] M. Albright, J. Kapusta and C. Young, *Phys. Rev. C* **90**, 024915 (2014) [*arXiv:1404.7540 [nucl-th]*].
 - [22] A. Miyahara, Y. Torigoe, H. Kouno and M. Yahiro, *Phys. Rev. D* **94**, 016003 (2016) [*arXiv:1604.05002 [hep-ph]*].
 - [23] M. Asakawa, T. Hatsuda, *Phys. Rev. B* **55**, 7 (1997).
 - [24] L. Landau and E. Lifshitz, *Statistical Physics* (Pergamon, New York, 1980).
 - [25] S. Borsányi *et al.*, *Nature* **539**, 69 (2016) [*arXiv:1606.07494 [hep-lat]*].
 - [26] R. Bellwied, S. Borsányi, Z. Fodor, S. D. Katz, A. Pasztor, C. Ratti and K. K. Szabo, *Phys. Rev. D* **92**, 114505 (2015) [*arXiv:1507.04627 [hep-lat]*].
 - [27] S. Borsányi, Z. Fodor, S. D. Katz, S. Krieg, C. Ratti, and K. K. Szabo, *JHEP* **01**, 138 (2012).
 - [28] S. Borsányi, G. Endrödi, Z. Fodor, S. D. Katz, S. Krieg, C. Ratti, and K. K. Szabo, *JHEP* **08**, 053 (2012).
 - [29] N. Haque, J. O. Andersen, M. G. Mustafa, M. Strickland and N. Su, *Phys. Rev. D* **89**, 061701 (2014) [*arXiv:1309.3968 [hep-ph]*]; N. Haque, A. Bandyopadhyay, J. O. Andersen, M. G. Mustafa, M. Strickland and N. Su, *JHEP* **1405**, 027 (2014) [*arXiv:1402.6907 [hep-ph]*].
 - [30] H. Kouno, T. Makiyama, T. Sasaki, Y. Sakai, and M. Yahiro, *J. Phys. G: Nucl. Part. Phys.* **40**, 095003 (2013).
 - [31] K. V. Olive *et al.* (Particle Data Group), *Chin. Phys. C* **38**, 090001 (2014).
 - [32] S. Borsányi, G. Endrodi, Z. Fodor, A. Jakovac, S. D. Katz and K. K. Szabo, *JHEP* **1007**, 056 (2012).
 - [33] S. Borsányi, G. Endrodi, Z. Fodor, A. Jakovac, S. D. Katz, S. Krieg, C. Ratti and K. K. Szabo, *JHEP* **1011**, 077 (2010) [*arXiv:1007.2580 [hep-lat]*].
 - [34] Y. Aoki, S. Borsányi, S. Dürr, Z. Fodor, S. D. Katz, S. Krieg, and K. K. Szabó, *JHEP* **06**, 088 (2009).
 - [35] S. Ejiri, *Phys. Rev. D* **77**, 014508 (2008) [*arXiv:0706.3549 [hep-lat]*].